Modeling of a Cast Aluminum Wheel for Crash Application

Yann Léost, Alixa Sonntag, Thomas Haase

Fraunhofer Institute for High-Speed Dynamics, Department for Material Dynamics, Ernst-Mach-Institut, EMI, Eckerstraße 4, 79104 Freiburg, Germany

1 Introduction

Wheels may be subjected to severe loading in case of a vehicle crash and often play a predominant role in vehicle safety, especially in frontal load case such as the small overlap [1]. In this specific scenario, the front parts that should absorb the crash energy (bumper, crash box, frame rail) are less involved, resulting in a significant amount of energy directly transmitted to the wheel that may intrude in the passenger compartment and may cause severe injuries to the occupants. However, references in literature concerning wheel modeling deal mainly with vehicle dynamics and NVH. Modeling of wheels for crash application requires information concerning the material used for the component and is usually not communicated to customers other than OEMs. The only official test concerning wheels under impact is described via SAE J175 [2]. However, taking a wheel load of 640 kg, the norm rule leads to an impact of 1.3 kJ which might not be as challenging as a wheel crash due to its comparatively low amount of kinetic energy. This motivates the present study, in which a representative cast aluminum wheel of 16” has been characterized and simulated through a reverse engineering process [3] as illustrated in Fig.1.

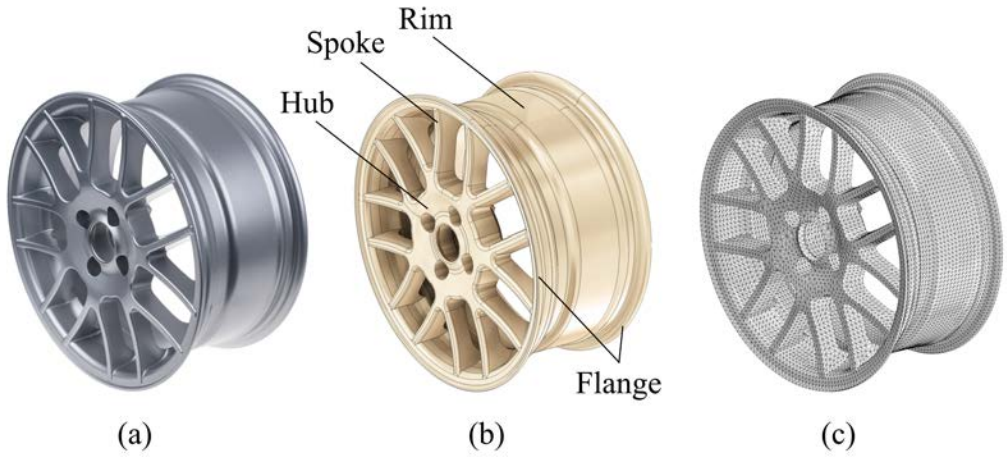

Fig.1: Reverse engineering process, (a) real wheel, (b) CAD model, (c) FEM model.

There are basically two main manufacturing processes concerning wheels: casting and forging. While the overall approach for the characterization and the modeling of a forged wheel remains the same, a higher strength and stiffer behavior for the latter manufacturing process can be expected. Section 2 presents the material characterization of the aluminum alloy of which the wheel is made. Coupons were directly extracted out of different locations and submitted to quasi-static and dynamic material tests. In addition, a microstructure analysis has been performed to investigate the possible difference in the metal structure. This section also describes the modeling of the aluminum behavior, using the commercial finite element (FE) code LS-DYNA and the damage model GISSMO (Generalized Incremental Stress-State dependent damage Model) [4]. Section 3 presents the crash test of the wheel and is followed by Section 4 which describes the numerical simulation of this specific scenario. The results are discussed in this section, before giving conclusions of this investigation.

2 Description of material characterization and modeling

2.1 Experimental setup

Aluminum coupons were extracted out of different locations in the wheel through an erosion process. Three different coupon dimensions have been chosen:

- 100 mm long tensile coupon, with a special section for gauge calibration, 7 mm width in the reduced section, 1.5 mm thick (a)
- 70 mm long tensile coupon, 7 mm width in the reduced section, 2.0 mm thick (b)
- 9 mm high cylinders for compression tests, 6 mm in diameter (c)

The extraction positions of the different coupons as well as an example of coupon extraction through erosion process are to be seen in Fig.2.

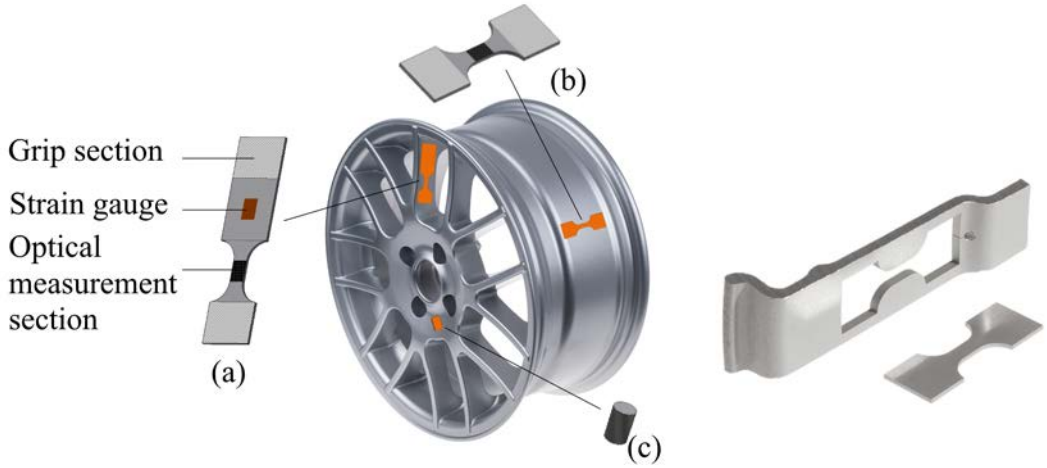

Fig.2: Left: Three different types of coupons, (a) tensile test from spokes, (b) tensile test from rim, (c) compression test from hub. Right: Tensile test coupon extracted from the rim through erosion process.

An overview of the characterization tests is given in Table 1. Each test has been repeated at least 3 times.

No.	Test type	Location	Strain rate (s^{-1})	Other
1	Tensile (a)	Spoke	10^{-3}	Strain gauge in reduced section, DIC[1]
2	Tensile (a)	Spoke	10^{-3}	Strain gauge for calibration, DIC[1]
3	Tensile (a)	Spoke	1	DIC[1]
4	Tensile (a)	Spoke	100	Strain gauge, DIC[1]
5	Tensile (b)	Rim	10^{-3}	DIC[1]
6	Compression (c)	Hub	10^{-3}	DIC[1]

[1]DIC: Digital Image Correlation

Table 1: Material characterization experiments

Quasi-static tests were performed at room temperature on a servohydraulic testing system Instron 8801. The haul-off speed was 0.024 mm/s for the spoke coupons, and 0.018 mm/s for those extracted from the rim, respectively. The position of the actuator and the tension force were recorded each time. Some specimens were specially prepared with a random gray-scale speckle pattern to post-process them by digital image correlation (DIC). The DIC was then performed with the software Aramis by GOM and provided information about local strain values in the section of interest. For some quasi-static experiments, small strain gauge rosettes were applied in the reduced section in order to

measure longitudinal and transverse strains and thus, determine the Poisson's ratio, along with an accurate value for Young's modulus.

Tensile tests at a strain rate of 1 s^{-1} were also performed on the same testing system. The haul-off speed for these tests was 24 mm/s. The tests at 2400 mm/s (strain rate of 100 s^{-1}) were performed on an Instron VHSJ4855 testing system. As those last tests might have led to large unwanted oscillations in force measurement, a calibration method was used to obtain an accurate force measurement. For this purpose, strain gauges were placed in the non-reduced section of the coupon, which is supposed to undergo only elastic deformations. However, due to the inhomogeneous character of the strain field in this section, the force measured by the actuator differs from the one derived from the gauge measurement, so the coefficient *k* that links both entities according to the following formula, had to be determined in the quasi-static experiments:

$$F_{actuator} = kF_{gauge} = kE\varepsilon_{gauge}A_0 \quad (1)$$

Fig.3 gives an example of the benefit of using the strain gauge method in comparison to a direct force measurement when the dynamic response is producing oscillations in force measurement.

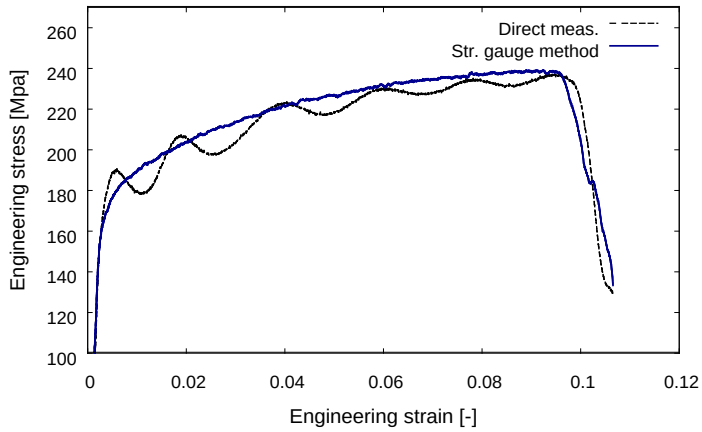

Fig.3: Comparison between direct force measurement and strain gauge method at a strain rate of 100 s^{-1}.

2.2 Characterization results

The microscopic analysis at different locations of the wheel revealed important discrepancies in the metal structure. Fig.4 presents different sizes of dendrites, which are multi-branching tree-like forms occurring during the crystallization of the metal. Dendrites in the rim are the smallest ones, with an average size of 400 µm, whereas the size of those from the spokes are 1000 µm and those in the hub, 1500 µm. Similar differences in wheel material locations were found in [5]. The main reason which can explain these differences is the manufacturing process in which the rim cools faster than the spokes and the hub, because of its comparatively small thickness. Large silicon phases are also clearly identifiable in the rim region, which is not the case for the other regions.

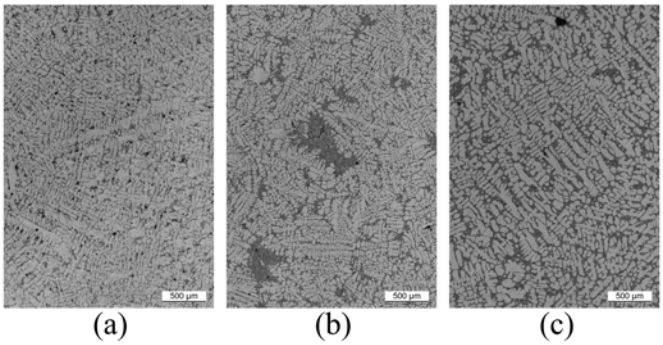

Fig.4: Microscope analysis of the spokes (a), the rim (b) and the hub (c).

Fig.5 presents the experimental curves of engineering stress vs. engineering strain for the extracted specimens. Fig.5 (a) gives an overview of the material strength difference between the spoke region and the rim region by quasi-static tensile tests. The rim region has a higher strength and ductility than the spoke region. Fig.5 (b) presents the results of tensile tests from the spoke region at different strain rates. The influence of strain rate on the material strength is marginal as the tests performed at 100 s^{-1} led to an increase of strength of only ~1.5% in comparison to the quasi-static experiments. However, a higher strain rate leads to an increase in the failure strain.

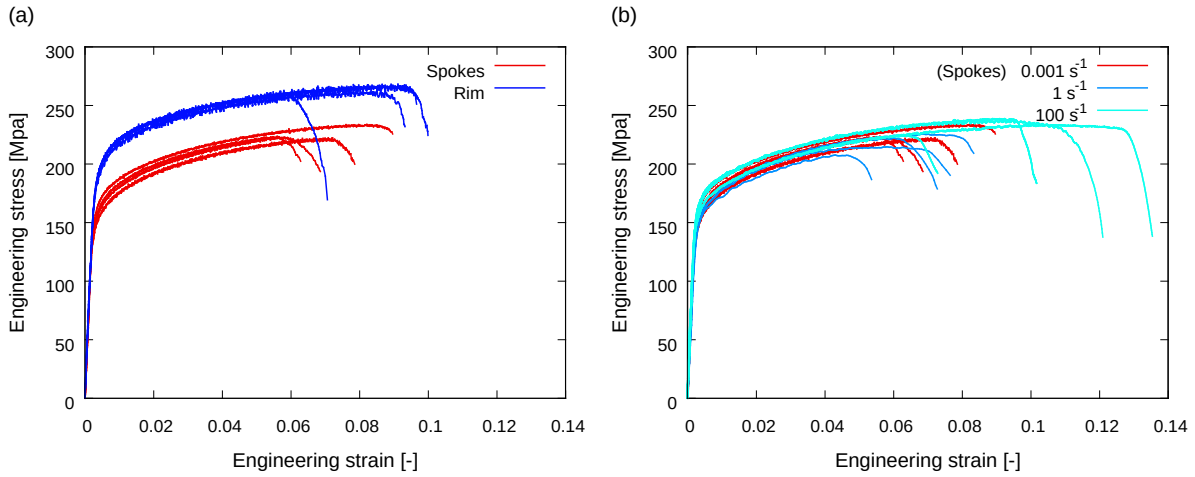

Fig.5: Engineering stress vs. engineering strain with regard to location for quasi-static tensile tests (a) and strain rate for specimens from the spokes (b).

The wide range of variation in the failure strain in tensile experiments conducted in the same extraction location is probably mainly due to the casting process which generates randomly placed cavities. Fig.6 shows the resulting pores that have been typically observed on coupons. Moreover, instead of a sudden failure, a onset of damage prior to failure appeared, which tends to make the use of a damage model more suitable for the following modeling activities. Experimental results were truncated just before exhibiting too large strain gradients during failure as the force and displacement measurements after this point might not be physically relevant. This question is discussed for simulation results in [6].
Eventually, no failure was observed in the compression tests. This motivates the further use of a material model taking into account the difference in failure strain depending on the stress state.

Fig.6: Example of tensile specimen (spokes) presenting some pores due to the casting process.

2.3 Material modeling

The material modeling was done using an elastic-plastic material model (***MAT_24**) with tabulated yield curves, taking into account the small strain rate dependency showed in the material characterization. Considering the true stress and true plastic strain that were extracted from the tensile tests, a parametrized function based on the analytical hardening models from Swift and Voce was used to determine the correct post-localization hardening curve extrapolation.

In addition to this, a GISSMO damage model (***MAT_ADD_EROSION**, IDAM = 1) has been applied in order to take into account the following material characteristics:

- Progressive damage build up in the material
- Stress triaxiality dependence as the alloy revealed failure in tension and however only yield in compression
- Regularization to compensate for the differences in failure strain due to mesh size
- Influence of the strain rate on the failure strain

A full calibration of the damage model requires a variety of different tests that cover as many stress states as possible. All these tests were not conducted in the present study, as only coupons with a simple geometry as those for tensile or compression tests were first extracted from the wheel. Hence, experiments mainly delivered results in a load path between uniaxial and biaxial tension.
Mohr and Marcadet [7] proposed the three parameters Hosford–Coulomb (HC) criterion to describe the onset of shear and normal localization in metals under proportional loading. For plane stress conditions, the Lode angle parameter can be described as a function of the stress triaxiality. In this condition, it is possible to express the failure strain as a function of the stress triaxiality, (Fig.7, grey curves). Tests have been conducted on 2024-T351 aluminum [8] and a typical trend was found by plotting the equivalent plastic failure strain against the stress triaxiality, which corresponds to the shape given by the HC model by a=1 (Fig.7, a=1). Recent experiments on 6061-T6 aluminum on thin-walled tubular specimens [9] and under shear dominated loading thanks to an Arcan-like specimen [10] indicated a simpler trend however, where the strain to failure monotonically decreases with stress triaxiality, that might have the trend of the HC model by a=2 (Fig.7, a=2). The presence or not thereof, of a cusp at a stress triaxiality around 1/3 prompted discussions in this field. As the tests under shear loading and biaxial conditions were not carried out in this study, a simplified trend for the stress triaxiality dependence has been chosen (Fig.7, red curve). This model ensures that no failure occurs in compression and fits to the failure strains provided by the uniaxial experiments.

Model calibration has been performed using shell elements. It has the drawback of only being able to evaluate the material in plane stress conditions and thus, [11] recommends the use of solids in the calibration model if the component has to be simulated with solids later on. However, [6] presented an acceptable difference between a modeling with shells and with solids.

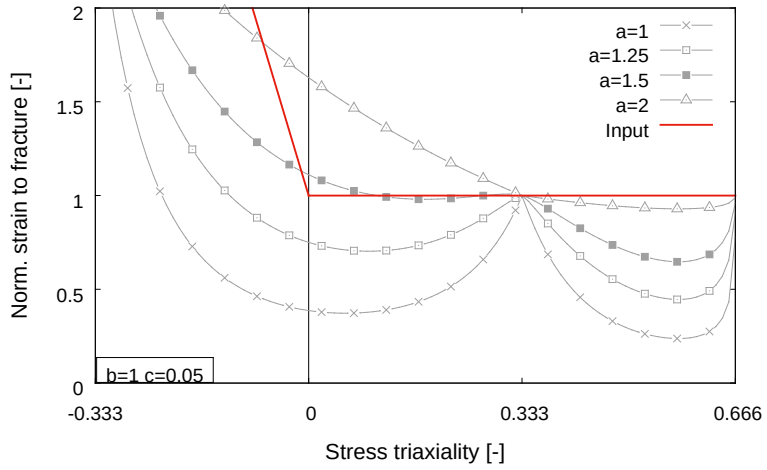

Fig.7: Parametrized Hosford-Coulomb (HC) model of the fracture envelope for plane stress loading (gray curves) and strain to failure vs. stress triaxiality input for the model (red curve).

First simulations were conducted with a shell element mesh size of 0.4 mm as a reference. Optical measurements of strain fields provided information concerning the local failure strain.

Thereafter, the damage DMGEXP and fading FADEXP exponents were calibrated to fit optimally with the experiments. The calibrated simulations were run with mesh sizes of 0.8 mm, 1.7 mm, 3.3 mm, and 6.7 mm, which enabled to determine the suitable regularization rule LCREGD in order to take the element size change into account. Results of the material characterization and regularized models are

presented in Fig.8. The parameter LCSRS enables the influence of the strain rate on the failure strain to be taken into account, by providing a scaling curve.

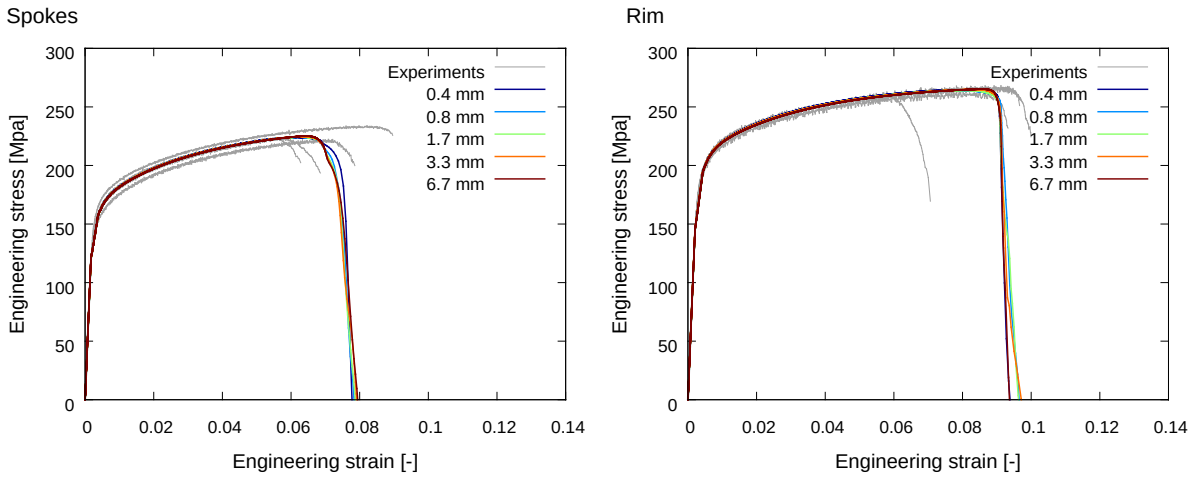

Fig.8: Regularized stress-strain curves for different element sizes, spokes (left), rim (right).

3 Experimental crash test setup

Two impact experiments have been conducted on the entire wheel at the component crash facility at Fraunhofer EMI. A preliminary simulation of a 40% overlap ODB frontal crash was conducted with the CCSA Toyota Yaris model [12] to determine the typical amount of energy that is absorbed by a simplified wheel model during such an event. From this preliminary simulation, it has been deduced that the wheel is subjected to an impact of approx. 8 kJ. The current facility is constrained to a minimum sled weight of 250 kg. Hence, the required velocity to submit the wheel to an impact with a comparable amount of energy is about 8 m/s.
Fig.9 shows the test setup for the wheel crash. The wheel was fixed horizontally (denominated X-direction) and the flat impactor has been accelerated thanks to an air-pressurized canon. The test was performed at room temperature. Displacement is measured using two sensors that are situated on the sled rails. Behind the wheel a steel plate is directly mounted onto a 3D force sensor. Each time, videos have been recorded by high speed cameras placed above and to the side of the wheel.

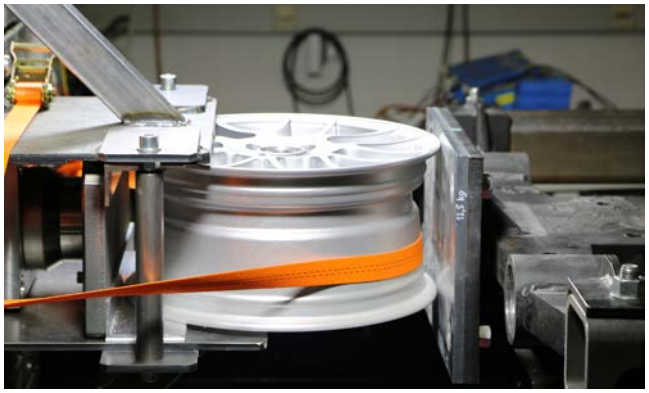

Fig.9: Experimental setup for wheel crash.

One of the main concerns was keeping the wheel firmly in its horizontal position in order to prevent it from tumbling or flying away, but at the same time, keeping the number of boundary constraints as low as possible in order not to affect the results of the intended loading by the selected fixation. Reproducibility and practicability have been considerably improved by using angles and Teflon sheets in the surrounding structure (Fig.9). Experimental results are presented in section 4.2.

4 Numerical model

4.1 Model setup

The first step consisted of the generation of a dependable CAD model of the rim, as the geometry strongly influences the simulation results [13]. Caliper gauge as well as 2D-scanning of cuts were performed (2D) to obtain the necessary information to build the CAD model. Some specific curvatures could be more precisely determined through a 3D scan and could be imported as splines in the CAD model.

Meshing is a crucial part of such a work and can strongly influence the model behavior depending on the element geometry and formulation that is used [14]. Meshing such geometries is much more convenient with tetrahedrons. However, it is generally recommended to use hexahedrons in such applications, as tetrahedrons tends to behave too stiffly. Two models have been generated with different meshes and element formulations (Fig.10). A description of these models is given in Table 2. In order to still achieve a reasonable computation time and allow the model to be used thereafter in vehicle crash simulations, the average element size was fixed to 5 mm.

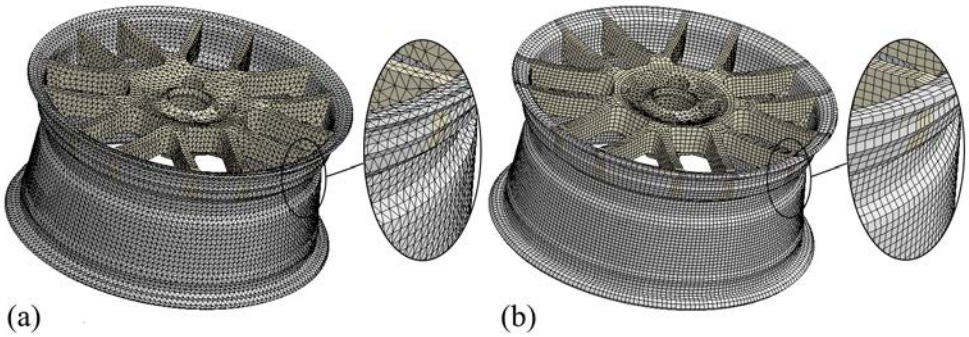

Fig.10: FEM models created for the component simulation, only tetrahedrons (a); hybrid model with hexa- and pentahedrons for rim and spokes and tetrahedrons for hub (b).

	Tetra model	Hybrid model
Rim	Tetrahedrons	Hexa- and pentahedrons
Spokes	Tetrahedrons	Hexa- and pentahedrons
Hub	Tetrahedrons	Tetrahedrons
Elements	63009	39920
Comp. time, 16 CPUs	37 min. No mass scaling	16 min. No mass scaling
Advantages	Easier mesh generation	Less elements than tetra model
Drawbacks	More elements than Hybrid	Time-consuming mesh generation

Table 2: Numerical model description

The following element formulations where used:

- Quadratic with nodal rotations and five point selective reduced integration for tetrahedrons (ELFORM = 4)
- Five point selective reduced integration for hexahedrons (ELFORM = 2)
- Two point selective reduced integration for pentahedrons (ELFORM = 15)

4.2 Model validation

The results are very similar in both experiments and the different phases described below were clearly identified there:

- A first force peak, which corresponds to the folding and the failure of the upper flange from 0 ms to 4 ms.
- The flat impactor then crushes the remaining rim and involves the spoke, creating plastic deformation in these parts and a bending of the rim, until the velocity reaches 0, at about 11 ms.
- Elastic spring back of the wheel and backward push of the impactor after 11 ms.

A comparison between experimental and numerical force displacement results is presented in Fig.11.

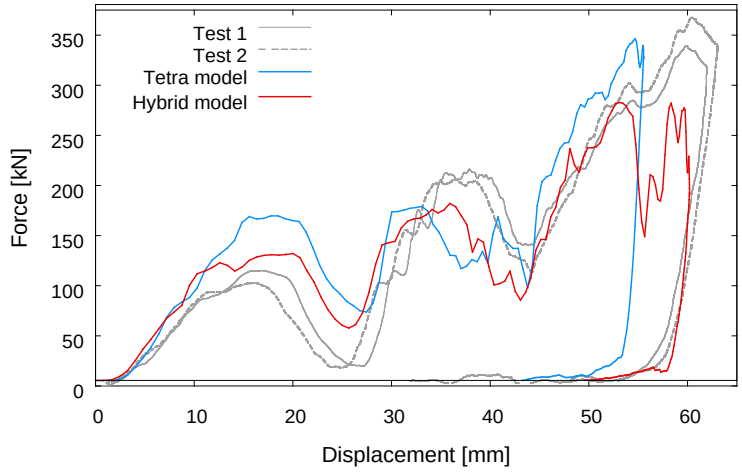

Fig.11: Force displacement results for crash test in comparison to simulation models.

Both models were able to reproduce the different phases of deformation and force peaks that have been previously described, but with some differences. The tetra model behaves too stiffly for the first peak but gives good results in terms of force level for the last peak. This element formulation is suitable for this type of application and was also recommended in [15]. However, the overall displacement with this model is slightly underestimated. The hybrid model gives a good prediction of the first peak and the total displacement forecasting with this model is excellent. However, the very last force peak is not reached with the hybrid model.
Considering the numerical results, the following conclusion can be drawn: The first phase of the crash scenario that mainly involves the rim and its failure was well predicted by the hybrid model, whereas the last peak at which the spokes and the hub are mostly involved was better described by the tetra model. Hence, a new model was considered with the following characteristics: modeling of the spokes and the hub is made of tetrahedrons whereas the rim is made of hexahedrons/pentahedron. Results for this new model are presented in Fig.12.

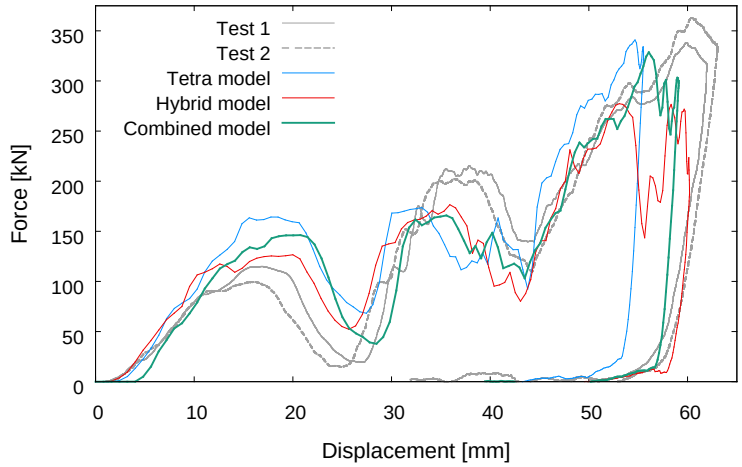

Fig.12: Simulation results concerning the new combined model in comparison to experiments and previous models.

The new combined model takes the advantages of the two previous models: the first force level and the overall displacement are better described than with the tetrahedron model and the last force peak could be much better caught in contrary to the hybrid (mostly hexa- and pentahedron) model. This new model has 36.486 elements and computes only in 16 minutes with 16 CPUs. An overview of the crash simulation sequences in comparison to the experimental test is presented in Fig.13. Displacement and failure modes could be well predicted by the numerical model.

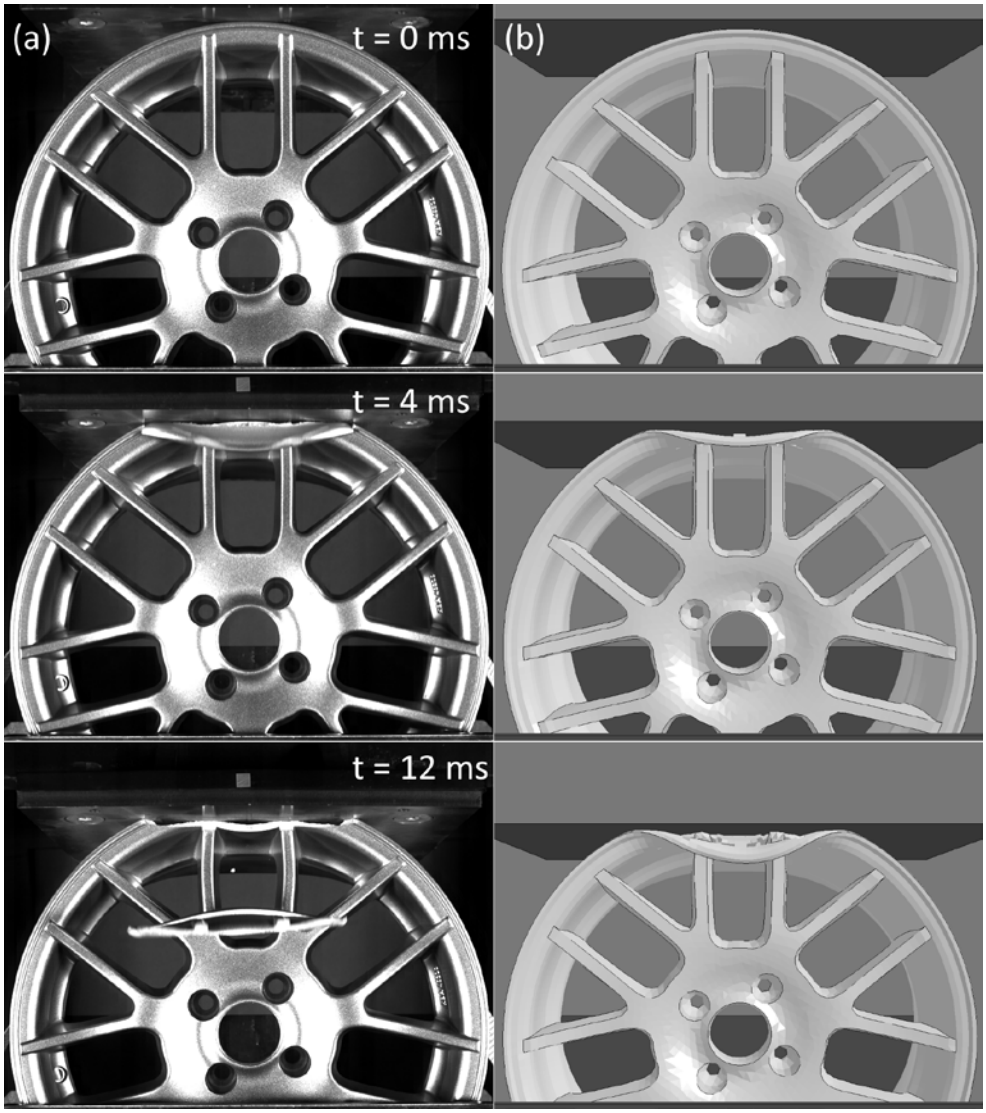

Fig.13: Wheel crash test (a) and comparison with numerical combined model (b).

5 Summary and outlooks

The main objective of the present research was to extract material properties from a conventional cast aluminum wheel through a reverse engineering process in order to validate the behavior of the full component in a crash simulation. A comprehensive set of tensile tests at various strain rates delivered enough information to calibrate both material and damage models for simulations. A simple stress triaxiality dependence was assumed based on experimental results and on literature. In addition, the model takes the onset of damage of the material, the element mesh-size regularization and the strain rate influence on the failure strain into account. Among the multiple choices in element formulation, two numerical models of the wheel were created, based on solid elements: one using exclusively tetrahedrons, and the other one using hexahedrons and pentahedrons for the rim and the spokes, and tetrahedrons for the hub. Advantages and drawbacks of both models have been discussed.

A detailed observation of both model behaviors lead to the design of a new “combined” model that takes the advantages of the two previous models by using hexa- and pentahedrons for the rim and tetrahedrons for the spokes and the hub.

Despite assumptions concerning the simplified stress triaxiality dependency and the characterization of the material under plane stress loading, a good prediction was obtained for the level of force and displacement for this “combined” model. Failure modes could be also well reproduced. Stress triaxiality dependency could be investigated retroactively: minor differences were observed by using the HC model with a=2, whereas the HC model with a=1 led to a collapse of the rim whereby the second and third force levels could not be reached.

The ongoing research at Fraunhofer EMI will gradually improve the model and answer a number of outstanding questions identified in the present paper. For instance, casting simulations and X-ray tomography could provide useful information concerning the material inhomogeneity resulting from the manufacturing process. A sub step validation on solid element level with a simple geometry could be valuable to determine the exact influence of the transition from a material characterization under plane stress condition to its use with solid elements.

6 Literature

[1] “Small Overlap Test Protocol”, Nov. 2016, www.iihs.org/.../Protocols/.../small_overlap_test_protocol.pdf.

[2] Society of Automotive Engineers: “Wheel Impact Test Procedures for Road Vehicles. SAE International”, SAE175.

[3] A. Sonntag, “Charakterisierung und Modellierung einer Fahrzeugfelge unter crashrelevanten Belastungen”, 2015, Bachelor Thesis at the Institute of Engineering Mechanics, Chair for Continuum Mechanics, Karlsruhe Institute of Technology (KIT).

[4] Livermore Software Technology Corporation: LS-DYNA Keyword User’s Manual Volume 1&2, 23.03.2015.

[5] R. Shang, W. Altenhof & al., “Wheel Impact Performance with Consideration of Material Inhomogeneity and a Simplified Approach for Modeling”, Journal of Crashworthiness, 10:2, 137-150.

[6] Callum J. Corbett et al., “Assessing and Validating the Crash Behavior of Securalex® HS, a High-Strength Crashworthy Aluminum Alloy, using GISSMO Model”, 14th International LS-DYNA Users Conference.

[7] D. Mohr and S.J. Marcadet, “Micromechanically-motivated phenomenological Hosford-Coulomb model for predicting ductile fracture initiation at low stress triaxialities”. International Journal of Solids and Structures (67-68), 2015.

[8] Bao Y. and Wierzbicki T., “On Fracture Locus in the Equivalent Strain and Stress Triaxiality Space”, International Journal of Mechanical Sciences, 2004, V.46, pp. 81-98.

[9] Haltom S.S., Kyriakides S. and Ravi-Chandar K., “Ductile Failure Under Combined Shear and Tension”, International Journal of Solids and Structures, 2013, V.50, pp. 1507-1522.

[10] Ghahremaninezhad A. and Ravi-Chandar K., “Ductile Failure Behavior of Polycrystalline Al 6061-T6 Under Shear Dominant Loading”, International Journal of Fracture, 2013, V.180, pp. 23-29.

[11] A. Haufe et al., „Predictive Fracture Modelling in Crashworthiness: A discussion of the Limits of Shell Discretized Structures“, LS-DYNA Forum 2016, Bamberg.

[12] “2010 Toyota Yaris Finite Element Model Validation Detail Mesh”, George Mason University, Center for Collision Safety and Analysis, CCSA, 2016, doi: 10.13021/G8CC7G.

[13] Russo C. J. Hrsg, “The Design and Processing of Cast Aluminum Wheels for Impact Performance”, SAE International, Warrendale, PA, 2001.

[14] T. Erhart, “Review of Solid Element Formulations in LS-DYNA, Review of Solid Element Formulations in LS-DYNA”, LS-DYNA Forum 2011.

[15] Burbulla F. et al., “Modellierung von Felge und Reifen zur Abbildung der Radkinematik im Fahrzeugcrash”, LS-DYNA Forum 2014, Bamberg.